MODELING THE INFRARED MAGNESIUM AND HYDROGEN LINES FROM QUIET AND ACTIVE SOLAR REGIONS

E. H. AVRETT

Harvard-Smithsonian Center for Astrophysics, 60 Garden Street, Cambridge, MA 02138, U.S.A.

E. S. CHANG

Department of Physics and Astronomy, University of Massachusetts, Amherst, MA 01003, U.S.A.

and

R. LOESER

Harvard-Smithsonian Center for Astrophysics, 60 Garden Street, Cambridge, MA 02138, U.S.A.

Abstract. The emission lines of Mg I at 7.4, 12.2, and 12.3 μm are now known to be formed in the upper photosphere; the line emission is due to collisional coupling of higher levels with the continuum together with radiative depopulation of lower levels. These combined effects cause the line source functions of high-lying transitions to exceed the corresponding Planck functions. However, there are uncertainties in a) the relevant atomic data, particularly the collisional rates and ultraviolet photoionization rates, and b) the sensitivity of the calculated results to changes in atmospheric temperature and density. These uncertainties are examined by comparing twelve calculated Mg I line profiles in the range 2.1–12.3 μm with ATMOS satellite observations. We show results based on different rates, and using different atmospheric models representing a range of dark and bright spatial features. The calculated Mg profiles are found to be relatively insensitive to atmospheric model changes, and to depend critically on the choice of collisional and photoionization rates. We find better agreement with the observations using collision rates from van Regemorter (1962) rather than from Seaton (1962). We also compare twelve calculated hydrogen profiles in the range 2.2–12.4 μm with ATMOS observations. The available rates and cross sections for hydrogen seem adequate to account for the observed profiles, while the calculated lines are highly sensitive to atmospheric model changes. These lines are perhaps the best available diagnostics of the temperature and density structure of the photosphere and low chromosphere. Further calculations based on these infrared hydrogen lines should lead to greatly improved models of the solar atmosphere.

Key words: atomic processes – infrared: stars – line: formation – Sun: atmosphere

1. Introduction

The Spacelab-3 ATMOS experiment of Farmer and Norton (1989) has obtained high quality disk-center solar spectra in the infrared wavelength range $\lambda = 2.1$–16.5 μm. These spectra include profiles of many atomic and molecular lines that originate from a wide range of depths in the photosphere, and provide the best observations available for determining the structure of the photosphere.

In this paper we compare calculated infrared profiles for both magnesium and hydrogen lines with the ATMOS observed profiles. The line profile calculations for these atoms must account for departures from LTE and are consequently more complex than LTE calculations of molecular lines. However, the Mg and H lines are formed over a greater range of depths than strong lines of CO and other molecules. Also, the H and CO lines have opposite temperature sensitivities, as shown in Sections 5 and 6.

D. M. Rabin et al. (eds.), Infrared Solar Physics, 323–339.

https://doi.org/10.1017/S0074180900124581 Published online by Cambridge University Press

The magnesium results given here represent a continuation of the results given in (1) our two previous papers, Chang *et al.* (1991, 1992); and (2) the extensive paper of Carlsson, Rutten, and Shchukina (1992a, hereafter CRS). See also Carlsson, Rutten, and Shchukina (1992b) and the paper of Rutten and Carlsson (1993) in these proceedings.

The hydrogen calculations reported here may be compared with the recent results of Carlsson and Rutten (1992, 1993).

2. Mg I Atomic Data

CRS have tested the sensitivity of their computed line profiles to changes in the various atomic data used in their calculation. They find that the results are most sensitive to changes in the Einstein A coefficients, but these are relatively well-established values. For high-l Rydberg lines the dipole matrix elements are essentially hydrogenic (see Hoang-Binh, 1993), while for low-l transitions the A coefficients have been independently calculated by several groups, giving values that are in very good agreement with each other.

The atomic processes that are next in importance are the bound-bound transition rates due to collisions with electrons. We and CRS both adopt the collision rates compiled by Mauas *et al.* (1988) for transitions between the low-lying levels.

For the remaining high-lying permitted transitions CRS use the impact parameter approximation of Seaton (1962). They assume no intersystem collisional coupling except for the intersystem rates given by Mauas *et al.* For each of the forbidden transitions within the singlet and triplet systems CRS assume "a collision strength of 5% of the closest permitted transition."

The procedure we use for the remaining high-lying permitted transitions is a choice of either 1) the same Seaton impact parameter formulae, or 2) the approximation by van Regemorter (1962) which gives collision rates that are larger by a factor of 3 or so. The rate that is calculated in either of these cases is proportional to the oscillator strength, f, of the transition. We treat all forbidden transitions in the same way as the remaining permitted transitions, but assume that $f = 0.1$. This way of treating the collision rates for forbidden transitions differs from that of CRS, and may partly explain why our computed profiles shown in Section 3 agree only approximately with those of CRS when we use the Seaton formulae. Another possible difference is that CRS included levels up to $n = 9$ while we have included additional hydrogenic levels up to $n = 15$.

Inelastic collisions with hydrogen atoms appear to have a much smaller effect than those with electrons, as discussed by CRS. For completeness, however, we have included the Mg-H collision rates from Kaulakys (1985) for transitions between the high-l (hydrogenic) levels of Mg I.

The calculated line profiles are also sensitive to the choice of photoionization rates. We find that different ways of treating photoionization from the $3p\,^3P^0$ level can significantly affect the solution. This rate depends on the photoionization cross section and on the radiation intensity in the $\lambda < 251$ nm wavelength region. We and CRS use similar cross section data. We use the results of Ueda, Karasawa, and Fukuda (1982) and CRS use the slightly higher values from Moccia and Spizzo

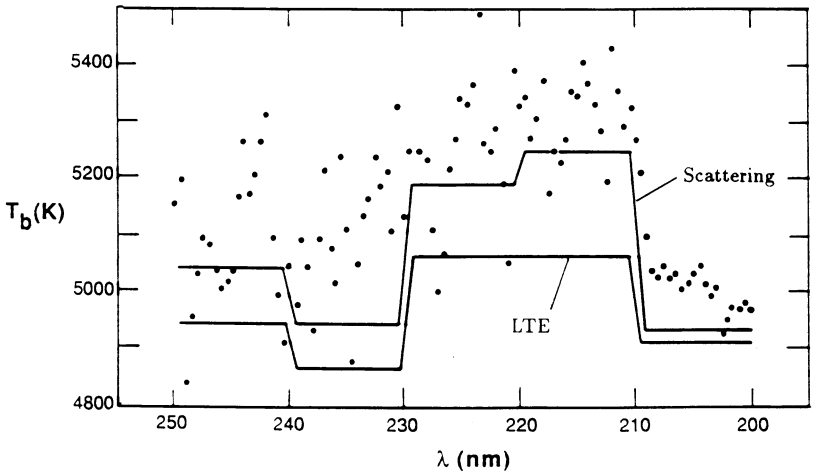

Fig. 1. Observed disk-center brightness temperature of the quiet Sun averaged over 0.5-nm intervals (dots), compared with calculated brightness temperatures averaged over 10-nm intervals.

(1988). The $\lambda < 251$ nm spectrum is filled with absorption lines, and both calculations use line opacity sampling based on the line lists of Kurucz (1991). CRS assume LTE in computing the $\lambda < 251$ nm radiation intensity. We show the results of assuming either a) approximate LTE, or b) that photons absorbed at line wavelengths are scattered so that the resulting mean intensity in the photoionization rate is less strongly coupled to the local Planck function than in LTE.

From a study of non-LTE line blanketing effects in the Sun, Anderson (1989) suggested the following expression for the depth-dependent scattering albedo σ for a given line: $\sigma = 1/(1 + C/A)$, where $C/A = Q \times (n_e/1.1 \times 10^{14})(\lambda/500)^3$. Here n_e is the electron number density at the given atmospheric depth, λ is the wavelength of the line in nm, and the parameter Q has the value 1 for ions, and 0.12 for atoms. An atomic line at $\lambda = 250$ nm formed at a depth where $n_e = 10^{13}$ cm^{-3} would have a scattering albedo $\sigma = 0.9986$. The scattering results we give in this paper use the value $Q = 0.12$. Our results assuming approximate LTE for the photoionizing lines are based on the value $Q = 10^4$, for which $\sigma = 0.0009$ in the above example.

We need to determine which of these two approximations ($Q = 0.12$ or 10^4 for scattering in the photoionizing lines) gives calculated mean intensities *vs.* depth in the range $\lambda < 251$ nm in better agreement with those in the solar atmosphere. The only comparison that can be made is between the calculated and observed emergent intensities in this wavelength range.

Figure 1 shows the brightness temperature corresponding to the observed disk-center intensity of the average quiet Sun plotted *vs.* wavelength. These are rocket observations by Kohl, Parkinson, and Reeves as tabulated by Vernazza, Avrett, and Loeser (1976). Figure 1 also shows the brightness temperatures corresponding to

https://doi.org/10.1017/S0074180900124581 Published online by Cambridge University Press

our calculated emergent intensities, averaged over 10 nm intervals, for the scattering ($Q = 0.12$) and LTE ($Q = 10^4$) line approximations discussed above. This comparison suggests that the $Q = 0.12$ scattering approximation for the photoionizing lines is better than assuming LTE for these lines.

3. Effect of Different Atomic Parameters

Scattering in the photoionizing lines is a non-LTE effect that enhances the emission in the Mg I 12 μm line. We find that using the Seaton collision rates with scattering in the $\lambda < 251$ nm lines gives excessive 12 μm emission, and that we obtain better agreement with the observations by using the larger van Regemorter collision rates. We will refer to these two cases as Se-Sct and VR-Sct, respectively.

Assuming LTE for the photoionizing lines tends to decrease the 12 μm emission so that using the Seaton rates gives better agreement with the observations in this case. Assuming LTE and the larger van Regemorter collision rates gives much less emission than is observed. These two cases are designated as Se-LTE and VR-LTE.

Figure 2 shows the observed ATMOS profiles for two Mg lines, and the computed profiles corresponding to the four cases referred to above. The two lines are the $7i$–$6h$ line at 811.6 cm^{-1} (12.32 μm) and the $6g$–$5f$ line at 1406.6 cm^{-1} (7.11 μm). The solid curve is the observed line in all four panels. The dotted profiles in panels *a* and *c* are the VR-Sct results, while the Se-LTE results are plotted with long-short dashes. These are the two cases in closest agreement with the observations. Panels *b* and *d* show the Se-Sct and VR-LTE results as long-dash and short-dash profiles, respectively. These results seem clearly inconsistent with the observations.

The profiles in Figure 2 correspond to disk center. Figure 3 shows the $7g$–$6f$ line at 848 cm^{-1} (11.79 μm) at $\mu = 0.14$ close to the solar limb. Here we compare the profile observed by Brault and Noyes (1983) with the computed VR-Sct and Se-LTE profiles (dots and long-short dashes, respectively). The VR-Sct results here are closer to the observations.

Given the results shown in Figures 1–3, we adopt the VR-Sct case for the purpose of further comparisons with the ATMOS profiles. The Se-LTE results in Figures 2 and 3 represent our attempt to duplicate the CRS calculations. However, CRS match the observed 12 μm line almost exactly while our Se-LTE profile is not a close fit. The results shown above therefore should not be regarded as a comparison of our results with those of CRS, but rather a comparison of the effects of using van Regemorter *vs.* Seaton collision rates, and of using scattering *vs.* LTE for the photoionizing lines.

4. Atmospheric Models

The computed profiles shown in Figures 2 and 3 were based on the atmospheric model for the average quiet Sun given by Maltby *et al.* (1986), hereafter called model C. Figure 4 shows the temperature as a function of height for this model and two others, A and F, discussed by Avrett (1985) and tabulated by Fontenla, Avrett, and Loeser (1992). In the upper photosphere and low chromosphere these three models have been constructed to account for the range of quiet-Sun Ca II H

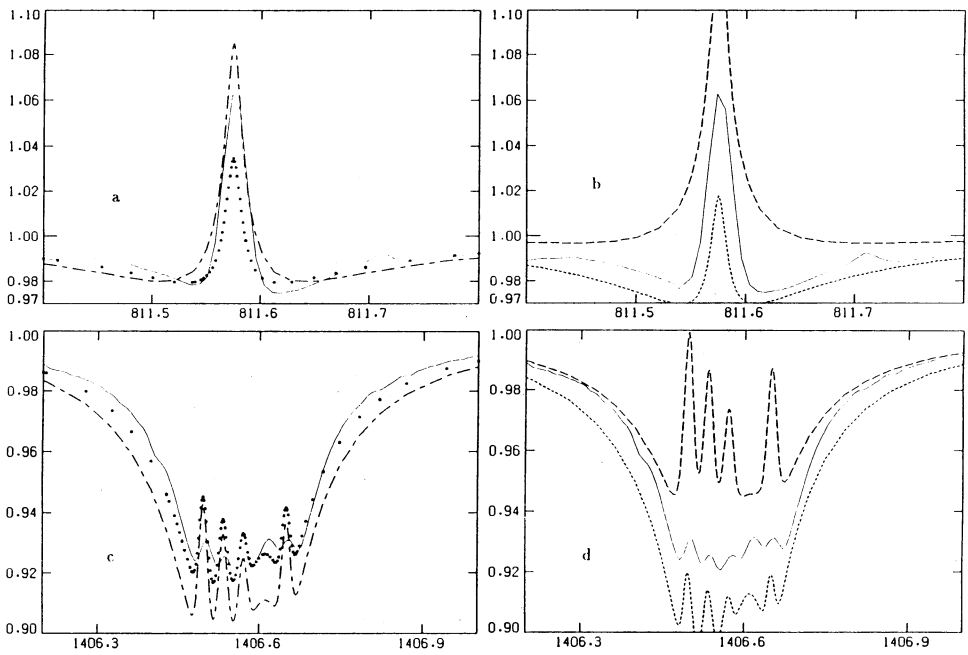

Fig. 2. Disk-center ATMOS profiles (solid lines) for the 811.6 and 1406.6 cm^{-1} Mg lines compared with the calculated results in four cases: Se-LTE (long-short dashes), VR-Sct (dots), Se-Sct (long dashes), and VR-LTE (short dashes).

https://doi.org/10.1017/S0074180900124581 Published online by Cambridge University Press

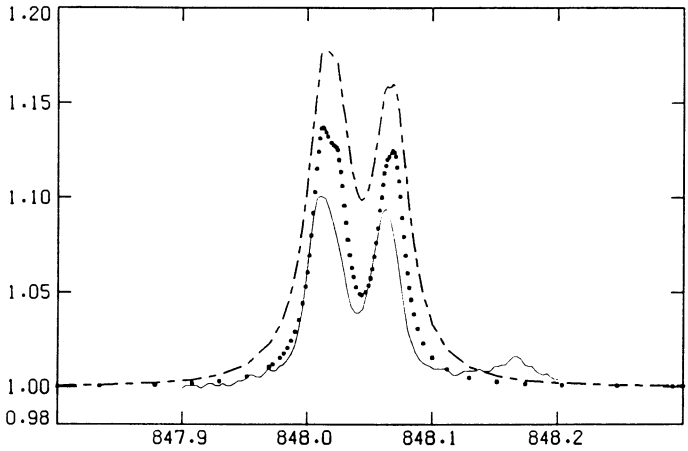

Fig. 3. Profile of the 848 cm^{-1} line at $\mu = 0.14$ observed by Brault and Noyes (solid line) and the calculated profiles in the two cases: Se-LTE (long-short dashes) and VR-Sct (dots).

line profiles observed at high spatial resolution by Cram and Damé (1983). Models A and F give H-line profiles that roughly match the profiles observed in the faintest 10% and the brightest 10% of quiet areas, while model C gives a computed H-line profile that roughly agrees with the observed spatially-averaged profile. Deeper in the photosphere, model C accounts for a range of infrared observations, as discussed by Maltby *et al.* (1986), and agrees with the model of Holweger and Müller (1974) derived from an analysis of a large number of lines throughout the visible spectrum. The models have an increase in temperature in the low chromosphere to account for the emission in the cores of the Ca II H and K lines and to account for the increase in the observed brightness temperature for $\lambda > 150$ μm in the far infrared and for $\lambda < 160$ nm in the ultraviolet. Models based on the CO lines, however, do not show a chromospheric temperature rise – see Ayres, Testerman, and Brault (1986). Note that the differences between models F and C occur deeper in the atmosphere than the differences between models A and C. The variations of models A and F relative to C are not well established. Very few unambiguous diagnostics are available to determine the properties of these colder and hotter component models. As shown in the next section the calculated infrared Mg lines have very little sensitivity to the differences between models A and F. However, a number of the hydrogen profiles shown later in Section 6 are highly sensitive to the differences between the three atmospheric models, and should be useful in obtaining improved models.

5. Calculated Mg I Lines

The Mg I term diagram in Figure 5 shows the lines considered in this section. These are the prominent Mg I lines that appear in the Farmer and Norton (1989) atlas.

https://doi.org/10.1017/S0074180900124581 Published online by Cambridge University Press

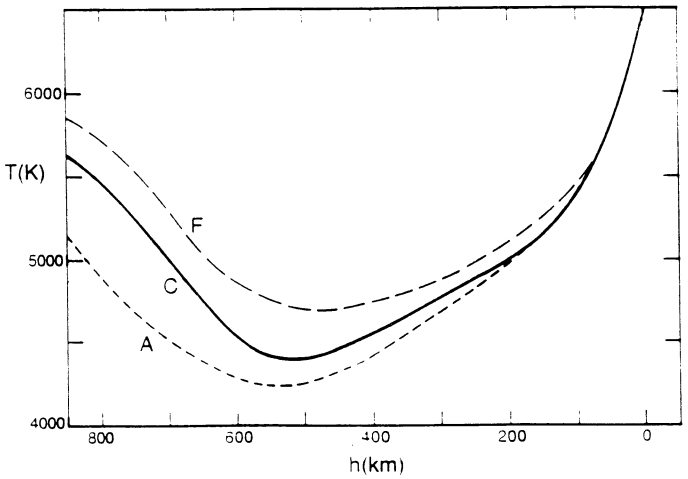

Fig. 4. Temperature *vs.* height for models A, C, and F.

The solid lines in panels *a* through *l* of Figure 6 are the observed profiles. The profiles computed from models A, C, and F are those plotted with short dashes, dots, and long dashes, respectively. All of these lines except those in panels *h* and *i* were discussed earlier by Chang *et al.* (1991, 1992).

From a theoretical viewpoint, the 958 cm^{-1} $7f$–$6\,^3D$ line in panel *i* is similar to the 848 cm^{-1} $7g$–$6f$ line in panel *j*, except that the 958 line is weaker, with three weak emission components instead of two blended pairs of stronger components in the case of the 848 line. The computed emission peaks in the 958 line are evidently too large. The 812, 818, 848, and 958 lines are successively weaker multiplet transitions between the $n = 7$ and $n = 6$ levels. As noted below, the emission we calculate is too small for the 812 line and too large for the 848 line. Correcting this disparity may also reduce the difference between the computed and observed 958 profiles.

The $7h$–$5g$ magnesium line in panel *h* is evident only as a broad depression. The two narrower features at 2166.03 and 2166.1 cm^{-1} are CO lines. Only in this panel of Figure 6 are the model A, C, and F results well separated, showing that the CO lines are much more sensitive to model changes than the Mg I lines.

In our calculations the groups of hydrogenic sublevels $5f$, g, $6f$, g, h, and $7f$, g, h, i in Figure 5 are each treated as single levels for the purpose of computing the non-LTE departure coefficients, b_n. Thus, the $n' - n$ line source function ($n' > n$) is

$$S_\nu = \frac{2h\nu^3/c^2}{(b_n/b'_n)\exp(h\nu/kT) - 1} \tag{1}$$

for the 1407 and 1356 lines in panels *f* and *g*, and for the 848, 818, and 812 cm^{-1} lines in panels *j*, *k*, and *l*. We account for the ν dependence of S_ν in equation (1) between the different multiplet lines. Note that $\exp(h\nu/kT)$ varies by the factor 1.01 between 848 and 812 cm^{-1} for $T = 5000$ K. Nevertheless, the central emission we calculate for the 812 line is less than observed, the calculated emission peaks

https://doi.org/10.1017/S0074180900124581 Published online by Cambridge University Press

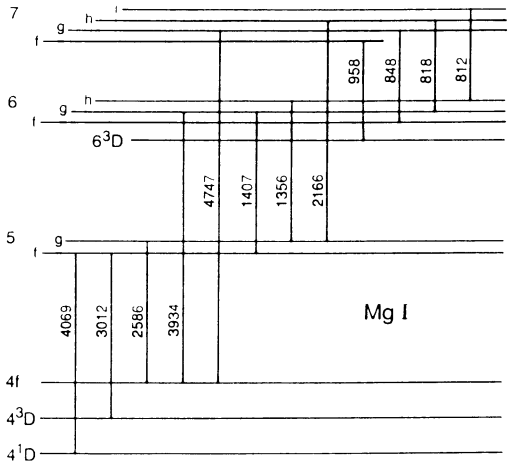

Fig. 5. Mg I term diagram showing the lines discussed in this paper.

for the 848 line tend to be higher than observed, while we obtain good agreement with the intermediate 818 line. CRS treat these sublevels as distinct levels, but they assume very large collision rates for nl'–nl transitions to obtain essentially a common b_n for each group. Thus we would expect the relative behavior of their calculated 812 and 848 lines to be similar to ours. However, they report very close agreement with the observations for both lines (see Rutten and Carlsson, 1993). The differences between our calculation and theirs need to be examined further.

We conclude from the present study that the infrared Mg lines are relatively insensitive to the choice of atmospheric parameters, but are highly sensitive to some of the atomic parameters used in the calculation, particularly the bound-bound collision rates and the degree of scattering in photoionizing lines. When we adopt a high degree of scattering for these lines, to be consistent with UV observations, we find that the van Regemorter collision rates give better agreement with infrared Mg observations than do the smaller Seaton values.

6. Hydrogen Lines

We have also computed the profiles of the infrared hydrogen lines that appear in the Farmer and Norton atlas. Because space is limited here we do not include a description of the various rates and cross sections used in our 15-level hydrogen calculation. These details will be provided in a forthcoming paper by Chang, Avrett, and Loeser (in preparation). Here we simply note that our rates and cross sections for hydrogen are basically the same as those described by Carlsson and Rutten (1992).

The hydrogen and magnesium calculations differ in that the hydrogen results show much less sensitivity to changes in the rates and cross sections. The profiles

https://doi.org/10.1017/S0074180900124581 Published online by Cambridge University Press

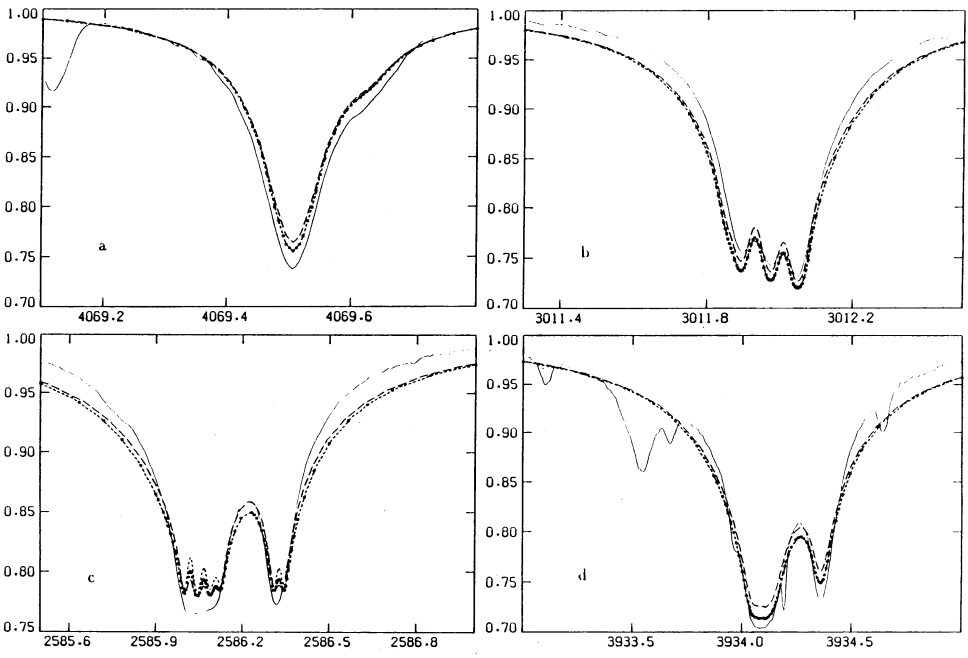

Fig. 6. Profiles of the 12 Mg I lines indicated in Figure 5. ATMOS observations (solid lines) compared with the profiles calculated from model A (short dashes), model C (dots), and model F (long dashes).

https://doi.org/10.1017/S0074180900124581 Published online by Cambridge University Press

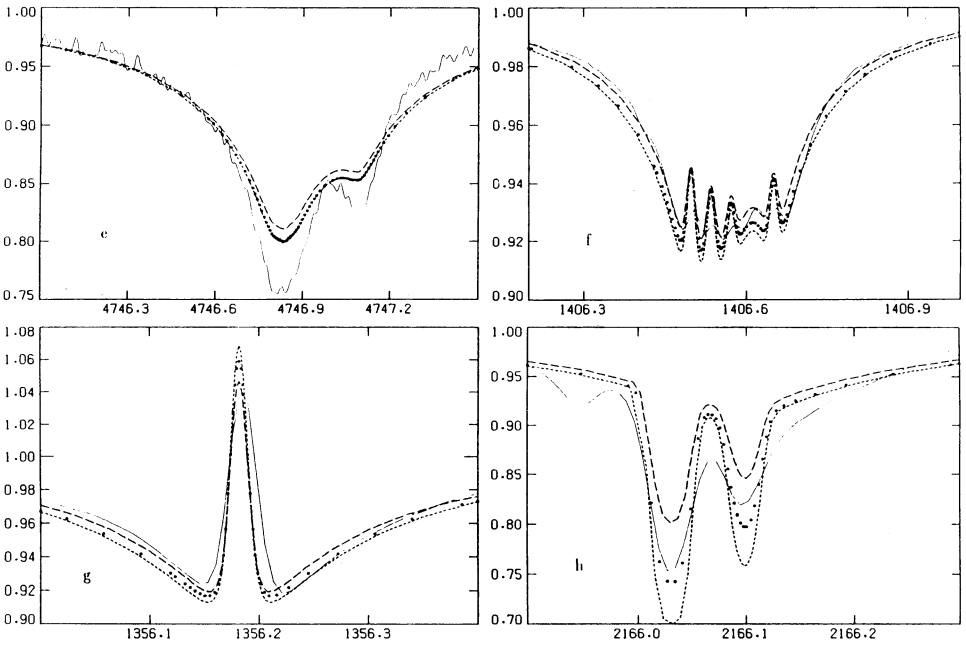

Fig. 6. *Continued.*

https://doi.org/10.1017/S0074180900124581 Published online by Cambridge University Press

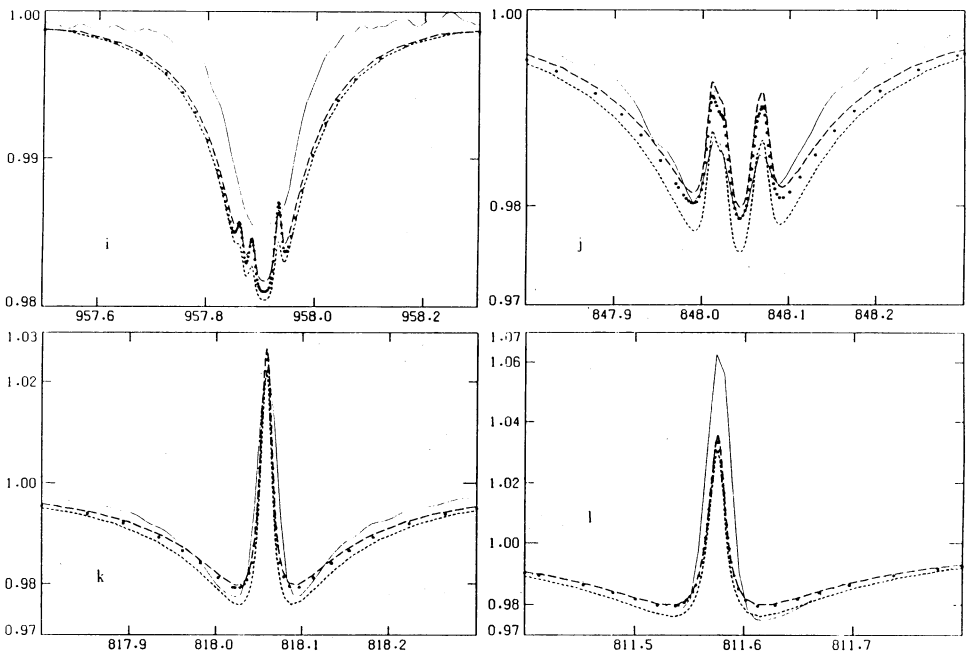

Fig. 6. ***Continued.***

https://doi.org/10.1017/S0074180900124581 Published online by Cambridge University Press

we show in Figure 7 below are essentially unaffected by changes in the bound-bound collision rates by factors of 2 to 4 (which occur when we use either the van Regemorter or Seaton rates instead of the values from Johnson 1972 that we use otherwise). Adopting LTE instead of scattering for the photoionizing lines also causes only small changes in the calculated hydrogen lines.

We show profiles for the hydrogen line transitions between levels with the following n'–n principal quantum numbers: 5–4, 6–4, 7–4; 6–5, 7–5, 8–5, 9–5, 10–5; 7–6, 8–6, 9–6; and 9–7. In each case we compare the disk-center profiles for models A, C, and F with the observed ATMOS profile. The results are shown in panels *a* through *i* of Figure 7.

The striking difference between these hydrogen profiles and those for Mg I in Figure 6 is the sensitivity of the hydrogen lines to the different atmospheric models. The model F profiles differ substantially from those calculated from models A and C. Note that except for the 7–6 and 9–7 lines, the model F central intensities are smaller than those for models A and C even though the model F temperatures are larger. In contrast, the CO-line model F intensities in Figure 6*h* are larger. The hydrogen lines behave in this way because the upper level number densities are highly sensitive to temperature. At 500 km, for example (see Fig. 4), the calculated number densities of the $n = 4$ level are 3.2×10^{1} (A), 1.3×10^{2} (C), and 1.1×10^{3} (F) cm^{-3} for models A, C, and F, respectively, and the values of $\tau_0(5\text{–}4)$, the 5–4 line center optical depth, are 0.023 (A), 0.21 (C), and 1.5 (F) at this height.

The 2586 cm^{-1} line of Mg I in Figure 6*c* is also a 5–4 transition (see Fig. 5), but the lower-level number density at 500 km in this case is about 1.7×10^{3} for all three models while the central optical depth of the Mg I 2586 line is 0.041 (A), 0.044 (C), and 0.047 (F) in the three cases.

For both H and Mg I, the $n = 4$ number density is closely related to the ion number density, because this level is so close to the continuum (0.85 eV in both cases). The proton number density is highly sensitive to the temperature in this region where hydrogen is almost completely neutral. In contrast, almost all magnesium is ionized so that the Mg II number density varies little with temperature.

In Figure 7*d* the 6–5 calculated profile for model C (and for model A) has a weak central emission feature which is due to $b_6 > b_5$ (see equation 2) in the upper photosphere and temperature minimum region, and not due to the chromospheric temperature rise. This calculated emission feature is analogous to the central peaks of the Mg I 6*g*–5*f* line at 1407 cm^{-1} (Fig. 6*f*). The central optical depth $\tau_0(6\text{–}5)$ of this hydrogen line has the value unity near 200 km in model C. The observed profile clearly does not show the central emission that we calculate in this case.

The deep absorption in the 6–5 model F profile is due to the much larger values of n_5, causing $\tau_0(6\text{–}5) = 1$ to occur near 800 km in the low chromosphere, and causing $b_6 \approx b_5 \approx 1$ in the upper photosphere. Furthermore, we find that $b_6 < b_5$ in the low chromosphere, which prevents the line source function from increasing as T increases in the 500–800 km region. We calculate a residual intensity at line center for model F of about 0.90, which is too low compared to the observed value of about 0.925. (The narrow central absorption feature in Figure 7*d* is not part of the solar line, but is due to H_2O absorption within the observing instrument.) We stated earlier that $\tau_0(5\text{–}4) = 1.5$ for model F at 500 km. $\tau_0(5\text{–}4) = 1$ occurs near

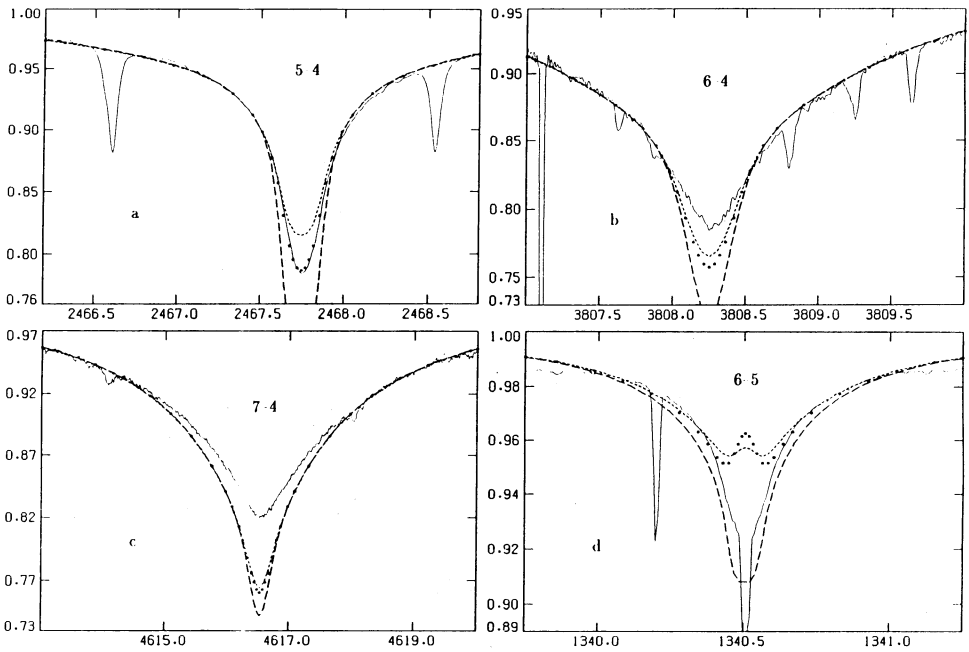

Fig. 7. Profiles of 12 hydrogen lines. ATMOS observations (solid lines) compared with the profiles calculated from model A (short dashes), model C (dots), and model F (long dashes).

https://doi.org/10.1017/S0074180900124581 Published online by Cambridge University Press

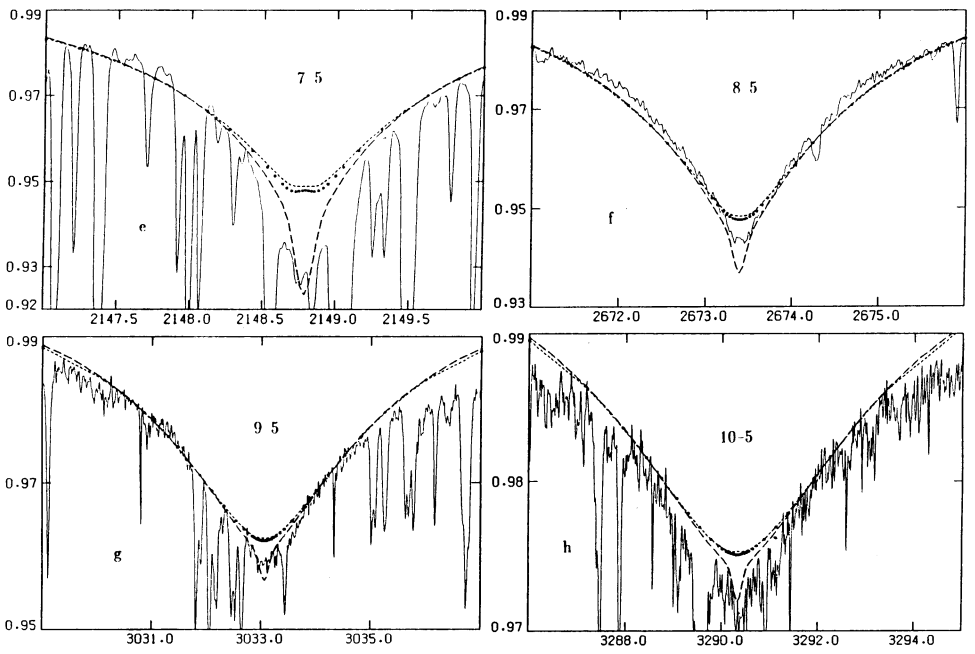

Fig. 7. *Continued.*

https://doi.org/10.1017/S0074180900124581 Published online by Cambridge University Press

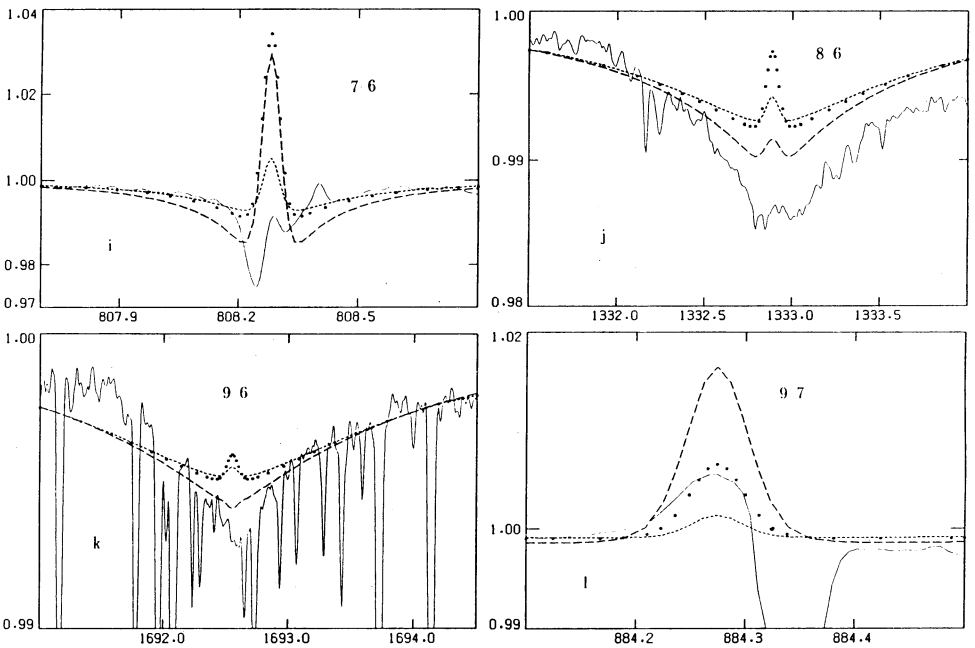

Fig. 7. *Continued.*

https://doi.org/10.1017/S0074180900124581 Published online by Cambridge University Press

850 km, where the temperature is about 1200 K above the minimum value. The 5–4 model F profile (Fig. 7*a*) does not have a central emission feature because $b_5/b_4 \approx 0.8$ at 850 km. The τ_0(7–6) values at 500 km are 0.030 (A), 0.22 (C), and 1.3 (F) which are similar to the τ_0(5–4) values of 0.023 (A), 0.21 (C), and 1.5 (F) at the same height. However, the 7–6 profiles in Figure 7*i* bear no resemblance to the 5–4 profiles in Figure 7*a*. These differences are due to two effects: 1) the line opacity is a much smaller fraction of the continuum opacity at 808 cm^{-1} than at 2468 cm^{-1}, and 2) at and just above the temperature minimum region the model calculations show that $b_5/b_4 < 1$ while $b_7/b_6 \geq 1$. The model F profiles of the 5–4 and 6–5 lines do not show a central emission feature because of the $b'_n/b_n < 1$ effect. All three computed 7–6 profiles show central emission due to both the chromospheric temperature rise and $b'_n/b_n > 1$.

The observed profile in Figure 7*i* shows a central H(7–6) emission feature together with a strong Mg I ($6d\,^1D$–$6p\,^1P$) absorption line just redward of the H(7–6) line center, and an emission line due to Si I ($7i[7\frac{1}{2}]$–$6h[6\frac{1}{2}]$) in the blue wing. The H(7–6) central emission we calculate is too large except perhaps for model A.

The 6–4 and 7–4 lines in Figures 7*b* and 7*c* are weaker than the 5–4 line but are less sensitive to atmospheric model changes. The 7–5, 8–5, 9–5, and 10–5 lines are weaker versions of the 6–5 line. The 8–6 and 9–6 lines are not only weaker than the 7–6 line but are less affected by the chromospheric temperature rise; the non-LTE effects giving central emission for models A and C are reduced in model F due to the higher densities.

Finally we consider the 9–7 line in Figure 7*l*. At 500 km the τ_0(9-7) values are 0.007 (A), 0.04 (C), and 0.2 (F), but $b_9/b_7 = 1.05$ (A), 1.03 (C), and 1.00 (F) in the three cases. The model A profile shows weak non-LTE emission while the model F emission is due to the chromospheric temperature rise. Both of these effects influence our model C profile, which matches the observed H(9–7) line rather well. The absorption feature at 884.35 cm^{-1} is a blend of two solar OH lines.

The 8–7, 9–8, 10–9, ... lines at wavenumbers 524.6, 359.7, 257.3, ... are emission lines, mainly due to the temperature rise. Brault and Noyes (1983) measured the profile of the 8–7 line at $\mu = 0.14$ near the limb and found the central emission to be 1.15 times the continuum. We compute 1.29 for model C, which is substantially larger. Boreiko *et al.* (1993) have detected the disk-center 8–7 line in emission from ground-based observations and have obtained profiles of the 12–11, 13–12, 14–13, and 16–15 emission lines from measurements at balloon altitudes. They find the central emission of the 14-13 line relative to the continuum to be about 1.10. Our calculated 14–13 profiles have central values 1.03 (A), 1.13 (C), and 1.30 (F), showing that only the model C result is consistent with the Boreiko *et al.* measurement.

7. Conclusions

We have compared ATMOS profiles of the Mg I and H lines in the 2.2–16.7 μm range with theoretical profiles calculated from three given atmospheric models corresponding to faint, average, and bright regions of the quiet Sun. The calculated Mg I profiles have only minor differences due to these three models, but are quite

sensitive to the atomic rates and cross sections on which the calculation depends. The results suggest the possibility of using these detailed comparisons to accept or reject various alternative rates and cross sections.

The hydrogen profiles are less affected by uncertainties in the atomic data but are quite sensitive to changes in the atmospheric model parameters. We have interpreted the calculated results but have not made any changes in the atmospheric models to get better agreement with the observations.

The results shown here represent only the first step in utilizing the ATMOS infrared spectra to redetermine the structure of the solar photosphere and low chromosphere.

Acknowledgements

We are very grateful to Dr. R. L. Kurucz for providing the calibrated ATMOS profile data shown here. This work has been supported by NASA Grant NSG-7054.

References

Anderson, L. S.: 1989, *Astrophys. J.* **339**, 558.
Avrett, E. H.: 1985, in B. W. Lites (ed.), *Chromospheric Diagnostics and Modelling*, National Solar Observatory, Sunspot, NM, p. 67.
Ayres, T. R., Testerman, L., and Brault, J. W.: 1986, *Astrophys. J.* **304**, 542.
Boreiko, R. T., Clark, T. A., Naylor, D. A., and Busler, J.: 1993, these proceedings.
Brault, J. and Noyes, R.: 1983, *Astrophys. J.* **269**, L61.
Carlsson, M., and Rutten, R. J.: 1992, *Astron. Astrophys.* **259**, L53.
Carlsson, M., and Rutten, R. J.: 1993, these proceedings.
Carlsson, M., Rutten, R. J., and Shchukina, N. G.: 1992a, *Astron. Astrophys.* **253**, 567 (CRS).
Carlsson, M., Rutten, R. J., and Shchukina, N. G.: 1992b, in M. S. Giampapa and J. A. Bookbinder (eds.), *Cool Stars, Stellar Systems, and the Sun, Seventh Cambridge Workshop*, Astron. Soc. Pacific, San Francisco, p. 518.
Chang, E. S., Avrett, E. H., Mauas, P. J., Noyes, R. W., and Loeser, R.: 1991, *Astrophys. J.* **379**, L79.
Chang, E. S., Avrett, E. H., Mauas, P. J., Noyes, R. W., and Loeser, R.: 1992, in M. S. Giampapa and J. A. Bookbinder (eds.), *Cool Stars, Steller Systems, and the Sun, Seventh Cambridge Workshop*, Astron. Soc. Pacific, San Francisco, p. 521.
Cram, L. E., and Damé, L.: 1983, *Astrophys. J.* **272**, 355.
Farmer, C. B., and Norton, R. H.: 1989, *A High-Resolution Atlas of the Infrared Spectrum of the Sun and the Earth Atmosphere from Space*, NASA Ref. Pub. 1224, Vol. 1.
Fontenla, J. M., Avrett, E. H., and Loeser, R.: 1992, *Astrophys. J.*, in press.
Hoang-Binh, D.: 1993, these proceedings.
Holweger, H., and Müller, E. A.: 1974, *Solar Phys.* **39**, 19.
Johnson, L. C.: 1972, *Astrophys. J.* **174**, 227.
Kaulakys, B.: 1985, *J. Phys. B.*, **18**, L167.
Kurucz, R. L.: 1991, in L. Crivellari, I. Hubeny, and D. G. Hummer (eds.), *Stellar Atmospheres: Beyond Classical Models*, p. 441.
Maltby, P., Avrett, E. H., Carlsson, M., Kjeldseth-Moe, O., Kurucz, R. L., and Loeser, R.: 1986, *Astrophys. J.* **306**, 284.
Mauas, P. J., Avrett, E. J., and Loeser, R.: 1988, *Astrophys. J.* **330**, 1008.
Moccia, R., and Spizzo, P.: 1988, *J. Phys. B.*, **21**, 1133.
Rutten, R. J., and Carlsson, M.: 1993, these proceedings.
Seaton, M. J.: 1962, *Proc. Phys. Soc. London*, **79**, 1105.
Ueda, K., Karasawa, M., and Fukuda, K.: 1982, *J. Phys. Soc. Japan*, **51**, 2267.
van Regemorter, H.: 1962, *Astrophys. J.* **136**, 906.
Vernazza, J. E., Avrett, E. H., and Loeser, R.: 1976, *Astrophys. J. Suppl.* **30**, 1.